Elastic Instability in α-Quartz under Pressure

N. Binggeli and James R. Chelikowsky
Department of Chemical Engineering and Materials Science, University of Minnesota and Minnesota Supercomputer Institute, Minneapolis, Minnesota 55455
(Received 30 July 1992)

The elastic properties of α-quartz are studied as a function of pressure using both a classical interatomic potential, and a first-principles pseudopotential approach. In both cases, we find that the structure becomes mechanically unstable at about 30 GPa. Our results suggest that the amorphization of quartz observed experimentally in this pressure range is triggered by the onset of a lattice shear instability. We analyze the microscopic origin of the elastic softening, and relate it to the presence of an oxygen close-packed cubic arrangement in the quartz high-pressure structure. A change in the Si coordination is found to be intimately related to the shear instability.

PACS numbers: 61.50.Ks, 62.20.Dc, 62.50.+p

Pressure-induced amorphization has been observed recently in a number of ionic crystals [1,2]. These solids vitrify when they are compressed at a sufficiently low temperature to kinetically inhibit crystallization to the stable high-pressure phase. Among the most studied of these solids is α-quartz. At room temperature, and for pressures up to 3 GPa, α-quartz is the stable form of silica. At higher pressures, the quartz structure persists as a metastable state, which gradually transforms to an amorphous form in the 25–35-GPa range [3]. A similar amorphization under hydrostatic compression was reported for other oxides with the quartz structure such as [1,4] $AlPO_4$ and GeO_2. Considerable interest currently exists in such direct crystalline-to-amorphous transitions because of their technological potential for production of bulk amorphous materials, as well as their fundamental importance in geophysics. The driving force for these transformations, however, is not well understood.

Amorphous materials are normally produced by cooling a liquid sufficiently fast to prevent crystallization. Pressure-induced amorphization is a more puzzling process, and the resulting amorphous solids often exhibit peculiar properties, such as the so-called "memory effect." For instance, amorphous berlinite ($AlPO_4$) obtained by hydrostatic compression reverts to the quartz structure, upon release of the pressure, with the same crystal orientation as before the amorphization [1]. Silica remains amorphous when the pressure is released, but the material is anisotropic, having retained the "memory" of the quartz crystallographic orientation [5]. Such effects suggest that the atomic disorder produced by pressure in these solids derives from a relatively small perturbation of the quartz crystalline structure.

The objective of this Letter is to identify the driving force behind the amorphization of α-quartz. In pioneering studies by Tsuneyuki and co-workers [6] and Tse and Klug [7], molecular-dynamics simulations based on pair potentials were used to investigate the effect of pressure on quartz. In both simulations, a structural transition occurred near the experimental amorphization pressure. Tsuneyuki and co-workers [6] observed a transition to a sixfold-coordinated Si crystalline structure, and in some of the simulation runs, to mixed fourfold-sixfold-coordinated Si crystalline structures. Tse and Klug [7], performing the simulation in a larger period supercell with slightly different values of the potential parameters, reported a transition to a "disordered" structure. However, by simply following the time evolution of the structural properties at the transition pressure [7], such studies did not identify the physical driving force responsible for the quartz amorphization. Here we focus on what triggers the transition, and show why the crystal collapses at that pressure. The sudden decrease of the Born elastic modulus $B_2=(c_{11}+c_{12})c_{33}-2c_{13}^2$, displayed in Ref. [7] as a function of time at the critical pressure, and the violation of the condition $B_2>0$ pointed out by Tse and Klug appear to be the result of the transition rather than its cause [8].

In our calculations, we follow the theoretical pressure evolution of the quartz crystalline phase near and above the amorphization pressure. This approach yields information difficult or impossible to obtain through simulations or experiments, and demonstrates that the quartz crystalline structure is reaching the limit of its mechanical stability, i.e., the spinodal boundary, near 30 GPa. The study of the structural trends across the stability limit allows us to clarify the microscopic process behind the instability. To investigate the elastic properties of quartz we use a classical force-field model as well as state-of-the-art first-principles calculations. An *ab initio* determination of the elastic properties of an oxide with a structure as complex as quartz is a serious computational challenge. Such a calculation, however, is important to put on a firmer ground. We use a simple ionic force-field model to explain the main features of the instability mechanism. In particular, the mixed covalent and ionic character of the Si-O bond in quartz is not captured by classical pairwise forces, and *a priori* the covalent nature of the bond may be important when dealing with the quartz amorphization.

The first-principles calculations are performed within the local-density functional (LDF) framework using the

pseudopotential plane-wave method [9]. We used the exchange-correlation potential of Ceperley and Alder [10] as parametrized by Perdew and Zunger [11] and norm-conserving soft pseudopotentials generated with the method of Troullier and Martins [12]. The technical details have been given elsewhere [13]. Stresses and forces are computed within the LDF using the reciprocal-space formulation of Ref. [14]. In the present study, plane waves up to a kinetic energy cutoff of 90 Ry were included in the basis set in order to have sufficiently accurate forces and stresses to determine the elastic properties. The Brillouin zone integrations were performed with a k-point mesh [15] ($2\times2\times2$) with displacement $(0,0,\frac{1}{4})$ in reciprocal lattice units. This grid yields two special k points for undistorted quartz. The k-point mesh chosen here has the unperturbed lattice symmetry, which insures a smooth transition from high-symmetry to low-symmetry lattices.

The force-field calculations are based on the same functional form for the interatomic potentials as employed in the simulation studies [6,7]. The two-body interactions are described by a Coulomb term and a short-range Born-Mayer correction. The results reported here have been obtained with the parameter values for the pair potentials proposed by Tsuneyuki, Tsukada, and Aoki [16]. These potentials give a relatively good qualitative description of the structural properties of a number of silica polymorphs [17]. For comparison, we also used the set of parameters proposed by van Beest and co-workers [16,18], and obtained results similar to those presented here for the pressure dependence of the quartz elastic properties.

For a solid under an initial hydrostatic pressure $p\neq0$, care must be taken in defining the elastic constants. The sets proposed in the literature are not unique [19]. The elastic constants c_{ij} calculated here are those defined from the stress-strain relation [19], and that appear in the equations of motion yielding the elastic-wave velocities. These c_{ij} are related to the energy variation to second order in the strain through [19]

$$\frac{\Delta E^{(2)}}{V_0}=-p\frac{\Delta V^{(2)}}{V_0}+\frac{1}{2}\sum_{i,j}c_{ij}\epsilon_i\epsilon_j\,. \tag{1}$$

A symmetric strain tensor ϵ is assumed in Eq. (1), and we use Voigt's notation [20].

$$\Delta V^{(2)}/V_0=\epsilon_1+\epsilon_2+\epsilon_3+\epsilon_2\epsilon_3+\epsilon_3\epsilon_1+\epsilon_1\epsilon_2-(\epsilon_4^2+\epsilon_5^2+\epsilon_6^2)/4$$

is the relative volume change to second order in the strain.

A necessary condition for a crystal to be mechanically stable is that the elastic-wave energy be positive, or equivalently, that the elastic constant matrix be positive definite (Born's criterion). For a trigonal structure, this results in the following conditions [21]:

$$\begin{aligned}B_1&=c_{11}-|c_{12}|>0\,,\\ B_2&=(c_{11}+c_{12})c_{33}-2c_{13}^2>0\,,\\ B_3&=(c_{11}-c_{12})c_{44}-2c_{14}^2>0\,.\end{aligned} \tag{2}$$

The first condition insures stability with respect to elastic waves in the x-y plane, i.e., perpendicular to the quartz c axis. The second condition is related essentially to dilatations, and insures a positive compressibility, while the third condition is associated with shear waves in planes different from the x-y plane. Specifically, $B_3=0$ corresponds [22] to a soft transverse acoustic mode with propagation and polarization vectors along one of the three equivalent directions in α-quartz, e.g., the x direction, and along a direction $\tilde{y}$ in the y-z plane at an angle $\beta=\arctan(-c_{44}/c_{14})$ to the c axis.

In Fig. 1, we show the theoretical pressure dependence of the B_1, B_2, and B_3, for pressures up to 50 GPa. The experimental values [23] at ambient pressure and 4 K are indicated by arrows. The zero-pressure elastic constants obtained from the pseudopotential calculations slightly overestimate the experimental results, an effect we attribute to the minimal k-point grid presently used in these heavy computations. The zero-pressure values obtained with the pair potentials by Tsuneyuki and co-workers underestimate, instead, the experimental data shown in Fig.

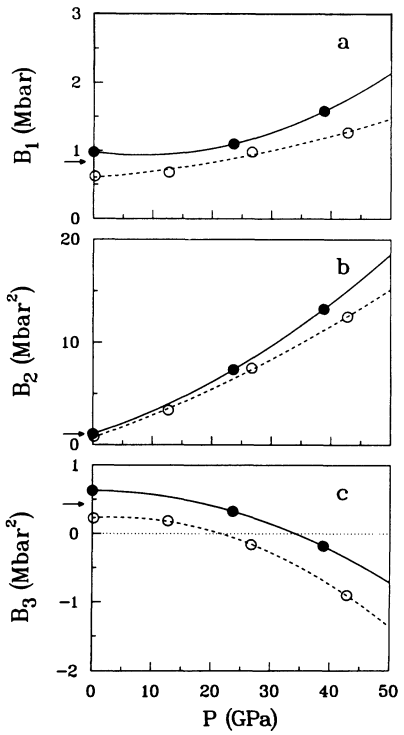

FIG. 1. Pressure dependence of the Born elastic moduli (a) $B_1=c_{11}-|c_{12}|$, (b) $B_2=(c_{11}+c_{12})c_{33}-2c_{13}^2$, and (c) $B_3=(c_{11}-c_{12})c_{44}-c_{14}^2$ for α-quartz. The result of the pair-potential and pseudopotential calculations are indicated by open and solid circles, respectively. The curves are guides to the eyes.

1. However, the *same* general pressure dependence of the elastic constants is obtained with the pseudopotential and pair-potential calculations. The first two moduli, B_1 and B_2, are positive in the whole pressure range shown in Fig. 1, and increase at high pressure. The change in the shear modulus B_1 is relatively small. B_2, however, increases drastically, changing by essentially 1 order of magnitude from ambient pressure to 40 GPa. The striking increase in B_2 is related to the decrease with pressure of the quartz compressibility. It reflects the increasing stiffness [24] of the Si-O-Si angle due to the Si-Si repulsion, when the bond bending approaches 120°.

The quartz instability is associated with B_3. In Fig. 1, B_3 decreases with pressure, and becomes negative at about 30 GPa, i.e., above 23 GPa using the empirical approach and below 35 GPa from the *ab initio* calculations. Using the potentials by van Beest and co-workers, B_3 is found to vanish at about 23 GPa. The two sets of interatomic potentials lead thus to an elastic instability at about the same pressure, which is responsible for the structural transformation of quartz observed in the molecular dynamics simulations [6,7]. This instability is associated with vanishing acoustic velocities, and leads to imaginary frequencies near Γ in the quartz phonon spectrum above the critical pressure. Large supercells are needed in simulations in order to reproduce the amorphization, and not the structural transformations reflecting an artificial periodicity. We note that contrary to what might be extrapolated [3] from the low-pressure behavior of the elastic constants, neither $c_{66}=\frac{1}{2}B_1$ nor c_{44} vanishes in the region of quartz amorphization (25–30 GPa). The elastic constant c_{66} increases above 10 GPa, while c_{44} decreases at high pressure, but vanishes only at about 50 GPa, i.e., far above the instability shown in Fig. 1(c). Thus, vanishing c_{66} or c_{44} is not the direct cause of the instability.

The pair-potential and pseudopotential approaches differ somewhat quantitatively with respect to the pressure scale, but reveal the same general microscopic process behind the quartz instability. The violation of the stability condition in Fig. 1(c) occurs when the oxygens in quartz approach a closed-packed body-centered-cubic (bcc) configuration [25]. This packing is the dominant mechanism which controls the structural behavior of quartz at high pressure. Since this oxygen cubic packing under pressure is a pure "Madelung effect" resulting from the minimization of the oxygen-oxygen repulsion, it appears more clearly why the simple pairwise-force model gives a correct qualitative description of the quartz high-pressure behavior and elastic instability.

The angle β between the c axis and the $\tilde{y}$ axis yielding the soft or softest shear $\epsilon_{x\tilde{y}}$ is about 40° at the transition, and decreases slightly at higher pressures. This angle saturates at about 35°, when the bcc packing is essentially completed ($P\approx 50$ GPa). The corresponding shear $\epsilon_{x\tilde{y}}$ has a simple interpretation in the bcc lattice. In Fig. 2 (upper section), we show the connection between the

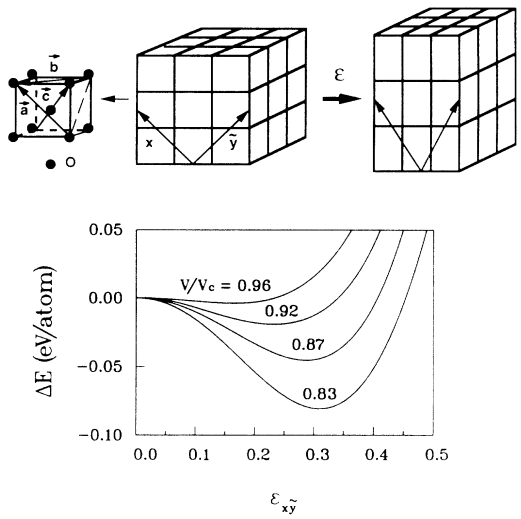

FIG. 2. Soft shear $\epsilon_{x\tilde{y}}$ on the oxygen body-centered-cubic (bcc) sublattice in the quartz high-pressure structure (upper panel). The Si are not equivalent in the small (SiO_2) oxygen bcc cells, and 27 of these cells are needed to form a periodic cubic cell of quartz. The hexagonal basis vectors **a**, **b**, and **c** of quartz correspond to two face diagonals and a body diagonal of the cube, respectively. The calculated energy relative to the unstrained configuration is given as a function of $\epsilon_{x\tilde{y}}$ (lower panel) for different volume ratio $V/V_c=0.96$, 0.92, 0.87, and 0.83, corresponding to pressures of 27, 33, 43, and 53 GPa, respectively.

quartz hexagonal basis vectors (**a**,**b**,**c**) and the oxygen cubic cell. For $\beta=\arccos(\sqrt{2/3})\approx 35.3°$, the shear $\epsilon_{x\tilde{y}}$ is ideally parallel to one of the three sets of planes forming the faces of the cube. The x and $\tilde{y}$ directions are face diagonals of the cube. The effect of the soft shear $\epsilon_{x\tilde{y}}$ is to elongate the cubic sublattice, as illustrated in Fig. 2. In the lower section of Fig. 2, we display the change in the total energy from the pair-potential calculations as a function of the $\epsilon_{x\tilde{y}}$ strain on the quartz unit cell. The calculations are performed at constant volume, and the results are shown for different volume ratios V/V_c, where $V_c=600$ a.u. is the critical unit cell volume for the quartz stability in the pair-potential calculation. For pressures above the critical pressure, a well clearly develops at finite strain $\bar{\epsilon}_{x\tilde{y}}$, showing the instability of quartz against the elongation of the oxygen cubic sublattice.

In Fig. 3, we compare for $V/V_c=0.91$ the microscopic atomic arrangement, obtained from the *ab initio* calculations, in the unstrained quartz structure and in the strained structure where $\epsilon_{x\tilde{y}}=0.3$. Microscopically, the effect of $\epsilon_{x\tilde{y}}$ is to open (close) the O-Si-O angles having the O atoms along (perpendicular) to the elongation axis. Such a deformation of the silica tetrahedron produces a displacement of the Si towards one of the nearby octahedral sites in the bcc lattice. The same effect is also found in the pair-potentials calculations. The displacement of the Si towards the octahedral site increases with $\bar{\epsilon}_{x\tilde{y}}$ and pressure. In both quartz-GeO_2 and -SiO_2, there is experimental evidence [26] for a change from a fourfold to a

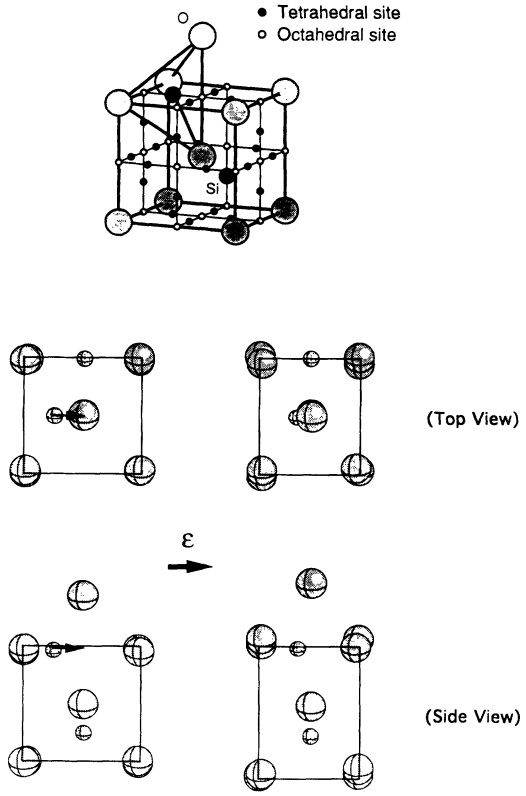

FIG. 3. Projection of the atomic arrangement in the quartz high-pressure structure for $V/V_c=0.91$ (left-hand side), and in the strained structure where a shear $\epsilon_{x\bar{y}}=0.3$ is applied on the quartz unit cell (right-hand side). The high-pressure bcc model of quartz and the tetrahedral and octahedral sites in the oxygen bcc lattice are illustrated in the upper section. The strain $\epsilon_{x\bar{y}}$ opens the O-Si-O angles with the O atoms along the elongation axis. This produces a displacement of the Si towards one of the nearby octahedral sites.

sixfold cation coordination above the amorphization pressure. We find this coordination change is intimately related to the shear instability.

In conclusion, using an *ab initio* pseudopotential approach we have shown that the experimentally observed amorphization of quartz occurs when the structure approaches a spinodal boundary associated with an elastic instability. Using a simple ionic model, we have analyzed the microscopic mechanism behind this instability, and shown its connection with a change in the Si coordination. Our calculations indicate that a shear instability can be the driving force toward a metastable crystal collapse, such as the quartz amorphization. This transformation is thus closely related to shear-melting [27] and martensitic [28] transitions.

We would like to acknowledge support for this work by the Division of Materials Research, Office of Basic Energy Sciences, U.S. Department of Energy under Grant No. DE-FG02-89ER45391 and by the Minnesota Supercomputer Institute. We also wish to thank H. King and N. Keskar for fruitful discussions.

[1] M. B. Kruger and R. Jeanloz, Science **249**, 647 (1990), and references therein.
[2] G. C. Serghiou, R. R. Winters, and W. S. Hammack, Phys. Rev. Lett. **68**, 3311 (1992), and references therein.
[3] R. J. Hemley, A. P. Jephcoat, H. K. Mao, L. C. Ming, and M. H. Manghnani, Nature (London) **334**, 52 (1988).
[4] G. H. Wolf, S. Wang, C. A. Herbst, D. J. Durben, W. F. Oliver, and K. Halvorson (to be published).
[5] L. E. McNeil and M. Grimsditch, Phys. Rev. Lett. **68**, 83 (1992).
[6] S. Tsuneyuki, Y. Matsui, H. Aoki, and M. Tsukada, Nature (London) **339**, 209 (1989).
[7] J. S. Tse and D. D. Klug, Phys. Rev. Lett. **67**, 3559 (1991).
[8] The drop of B_2 found in Ref. [7] is related to the volume change at the first-order transition. For a trigonal structure, the compressibility κ is given by $\kappa=(c_{11}+c_{12}-4c_{13}+2c_{33})/B_2$, and κ diverges (Fig. 1 in Ref. [7]) at the transition.
[9] J. Ihm, A. Zunger, and M. L. Cohen, J. Phys. C **12**, 4409 (1979); **13**, 3095 (1980).
[10] D. M. Ceperley and B. J. Alder, Phys. Rev. Lett. **45**, 566 (1980).
[11] J. P. Perdew and A. Zunger, Phys. Rev. B **23**, 5048 (1981).
[12] N. Troullier and J. L. Martins, Phys. Rev. B **43**, 1993 (1991).
[13] J. R. Chelikowsky, N. Troullier, J. L. Martins, and H. E. King, Jr., Phys. Rev. B **44**, 489 (1991); N. Binggeli, N. Troullier, J. L. Martins, and J. R. Chelikowsky, Phys. Rev. B **44**, 4771 (1991).
[14] O. H. Nielsen and R. M. Martin, Phys. Rev. B **32**, 3780 (1985).
[15] H. J. Monkhorst and J. D. Pack, Phys. Rev. B **13**, 5188 (1976); S. Froyen, Phys. Rev. B **39**, 3168 (1989).
[16] S. Tsuneyuki, Y. Tsukada, and H. Aoki, Phys. Rev. Lett. **61**, 869 (1988).
[17] N. R. Keskar and J. R. Chelikowsky, Phys. Rev. B **46**, 1 (1992).
[18] B. W. H. van Beest, G. J. Kramer, and R. A. van Santen, Phys. Rev. Lett. **64**, 1955 (1990).
[19] T. H. K. Barron and M. L. Klein, Proc. Phys. Soc. London **85**, 523 (1965).
[20] We use the notation: $\epsilon_1=\epsilon_{xx}$, $\epsilon_2=\epsilon_{yy}$, $\epsilon_3=\epsilon_{zz}$, $\epsilon_4=2\epsilon_{yz}$, $\epsilon_5=2\epsilon_{zx}$, and $\epsilon_6=2\epsilon_{xy}$.
[21] See, e.g., F. I. Fedorov, *Theory of Elastic Waves in Crystals* (Plenum, New York, 1968), p. 33.
[22] R. W. Terhune, T. Kushida, and G. W. Ford, Phys. Rev. B **32**, 8416 (1985).
[23] A. G. Smagin and B. G. Mil'shtein, Kristallografiya **19**, 832 (1975) [Sov. Phys. Crystallogr. **19**, 514 (1975)].
[24] K. L. Geisinger, G. V. Gibbs, and A. Navrotsky, Phys. Chem. Minerals **11**, 266 (1985).
[25] N. Binggeli and J. R. Chelikowsky, Nature (London) **353**, 344 (1991).
[26] J. P. Itie, A. Polian, G. Calas, J. Petiau, A. Fontaine, and H. Tolentino, Phys. Rev. Lett. **63**, 398 (1989); Y. Tsuchida, and T. Yagi, Nature (London) **347**, 267 (1990).
[27] D. Wolf, P. R. Okamoto, S. Yip, J. F. Lutsko, and M. Kluge, J. Mater. Res. **5**, 286 (1990).
[28] Y. Y. Ye, C.-T. Chan, K.-M. Ho, and B. N. Harmon, Int. J. Supercomput. Appl. **4**, 111 (1990).

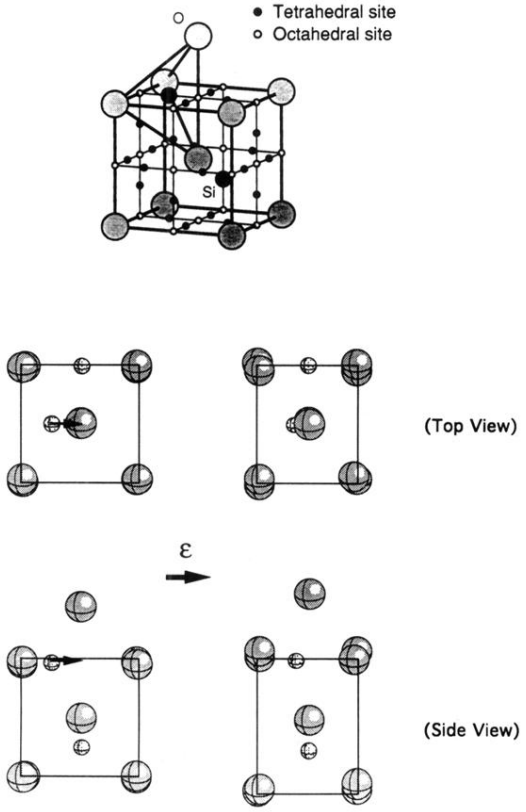

FIG. 3. Projection of the atomic arrangement in the quartz high-pressure structure for $V/V_c = 0.91$ (left-hand side), and in the strained structure where a shear $\epsilon_{x\bar{y}} = 0.3$ is applied on the quartz unit cell (right-hand side). The high-pressure bcc model of quartz and the tetrahedral and octahedral sites in the oxygen bcc lattice are illustrated in the upper section. The strain $\epsilon_{x\bar{y}}$ opens the O-Si-O angles with the O atoms along the elongation axis. This produces a displacement of the Si towards one of the nearby octahedral sites.